CERN – EUROPEAN ORGANIZATION FOR NUCLEAR RESEARCH

OPTIMISATION OF THE CLIC POSITRON SOURCE AT THE 1.5 TEV AND 3 TEV STAGES

Yongke Zhao[1,2], Andrea Latina[1], Steffen Doebert[1], Daniel Schulte[1], Lianliang Ma[2]

[1]CERN, Geneva, Switzerland
[2]Institute of Frontier and Interdisciplinary Science, Shandong University, Qingdao, China

Abstract

Positron source is very important for many accelerator experiments. The optimisation of positron source is therefore a crucial problem to be solved. In this report, a new simple, general and effective optimisation strategy is proposed, based on iterations of scan of free parameters, which has the advantage of easily handling realistic parametric problems. The new strategy in principle can be 25 times faster than the old optimisation method. The optimisation of the CLIC positron source at the 3 TeV and 1.5 TeV stages with the new strategy is presented. Positron yield is improved by 43% compared with previous studies, mainly due to the removal of the distance between the targets. The validation of the simulation code is carried out with a cross-check with the ILC positron source results. In addition, studies on mesh grid size for PEDD estimation and matching of positron beam to the latest design of the injector linac are also presented. Positrons can be transported in the matched injector linac almost without losses, with a final accepted yield of 2.14 e+/e-.

Geneva, Switzerland
24 September 2020

Optimisation of the CLIC positron source at the 1.5 TeV and 3 TeV stages

Yongke Zhao[1,2], Andrea Latina[1], Steffen Doebert[1], Daniel Schulte[1], and Lianliang Ma[2]

[1] *CERN, 1211 Geneva 23, Switzerland*

[2] *Institute of Frontier and Interdisciplinary Science, Shandong University, Qingdao 266237, China*

September 24, 2020

Abstract

Positron source is very important for many accelerator experiments. The optimisation of positron source is therefore a crucial problem to be solved. In this report, a new simple, general and effective optimisation strategy is proposed, based on iterations of scan of free parameters, which has the advantage of easily handling realistic parametric problems. The new strategy in principle can be more than 25 times faster than the old optimisation algorithm. The optimisation of the CLIC positron source at the 3 TeV and 1.5 TeV stages with the new strategy is presented. Positron yield is improved by 43% compared with previous studies, mainly due to the removal of the distance between the targets. The validation of the simulation code is carried out with a cross-check with the ILC positron source results. In addition, studies on mesh grid size for PEDD estimation and matching of positron beam to the latest design of the injector linac are also presented. Positrons can be transported in the matched injector linac almost without losses, with a final accepted yield of $2.14\,e^+/e^-$.

Keywords: CLIC; Positron source; Optimisation; PEDD

Contents

1 Introduction

Positron source is a very important part for many accelerator experiments, for example, electron-positron colliders and muon colliders with a positron-driven muon source. The optimisation of positron source is therefore an important task for those experiments. In this report, a new simple, general and effective strategy is introduced to optimise the positron source of the Compact Linear Collider (CLIC) experiment [1–6].

In the design and optimisation of the positron source, positron yield is always a very important discriminant quantity, which represents the positron production efficiency of the positron source. Since electrons are usually used to produce positrons by hitting tungsten or tungsten-alloyed targets, positron yield is usually defined as the ratio of the number of generated positrons to the number of injected electrons: $\eta_{e^+} = N_{e^+}/N_{e^-}$. However, only a fraction of positrons will be accepted by the pre-damping ring (PDR) or the damping ring (DR) that is located after the positron source. The yield of the accepted positrons is called the effective positron yield, $\eta_{e^+}^{\mathrm{eff}}$, which is the most important quantity to be optimised. Positron source with a higher effective positron yield is always prefered, due to its advantage of higher electron-positron conversion efficiency. But sometimes a high positron yield comes with a high primary electron energy which means a high cost, or a small electron beam spot size which causes a large energy deposition in targets and potential damage to the accelerator. In that case, a compromise between improving the positron yield and fulfilling the design and budgetary requirements is therefore necessary. To avoid the damage to the accelerator from the energy deposition, people put forward another important quantity, namely the peak energy deposition density (PEDD) [7]. For positron source, the PEDD is usually defined to be the maximum energy deposition of all particles per unit mass of the material per train of electron beam. The threshold of a safe PEDD with a long-term operation of the positron source without damaging the tungsten material is found to be 35 J/g [1]. To protect the targets from being damaged, a lower PEDD is always prefered.

In this report, a new optimisation strategy as well as its application to the CLIC positron source will be presented in Section 4. Nevertheless, the optimisation methodology or strategy can definitely be easily applied to any other experiments for the positron source design purpose. The CLIC positron source and the simulation are also briefly introduced in Section 2. Validation of the simulation code is performed by reproducing the International Linear Collider (ILC) [8] positron source simulation results and is presented in Section 3. A comparison with previous optimisation method and results are presented in Section 5. A study on PEDD is also performed to estimate the proper mesh grid size for energy deposition in the target simulation, which is presented in Section 6.

2 The CLIC positron source

The CLIC positron source, located at the beginning of the CLIC accelerator, is used to produce high-energy positrons for the collider. It is composed of an electron generator that is used to provide primary high-energy electrons, a hybrid target system that is used to convert electrons to positrons through interactions between electrons and the tungsten targets, a positron capture section which includes an adiabatic matching device (AMD) and a pre-injector linac, and finally an injector linac which is located in front of the pre-damping ring (PDR) and is used to accelerate positrons to a designed energy of 2.86 GeV.

A conventional primary electron-beam linac is used for the electron generator. Primary electrons are generated by an electron gun and thus accelerated by a following driver linac to the desired energy, 5 GeV. The hybrid target system consists of a thin crystal tungsten target and a thick amorphous tungsten target. As the high-energy electrons impinge the crystal tungsten target along the $\langle 111 \rangle$ axis, photons are generated

mainly through the axial channeling radiation from the relativistic electrons. Positrons are produced in an electromagnetic shower caused by the photons in the amorphous tungsten target, which is installed after the crystal target. Between the two targets, a dipole magnet with a strong magnetic field is placed to sweep away charged particles to reduce damage from energy deposition of particles to the second target.

The AMD is used to capture positrons from the targets, with a strong magnetic field at the beginning which is decreased adiabatically. The analytic formula [9] for the on-axis magnetic field description is:

$$B_z = \frac{B_0}{1 + \alpha z} \tag{1}$$

where, B_0 is the maximum value of the longitudinal on-axis magnetic field and α is a constant. For this purpose, the AMD is supposed to have a conical inner aperture, since the radius is inversely proportional to the square root of the longitudinal on-axis magnetic field [9]. To be consistent with the pre-injector linac, the inner aperture radius and the magnetic field at the end of AMD are $20\,\mathrm{mm}$ and $0.5\,\mathrm{T}$, respectively. The analytic AMD field B_z as a function of z can be demonstrated in Figure 1, where $B_0 = 6\,\mathrm{T}$ and the length of AMD is $20\,\mathrm{cm}$, according to the latest baseline of the CLIC positron source [4]. The AMD is expected to
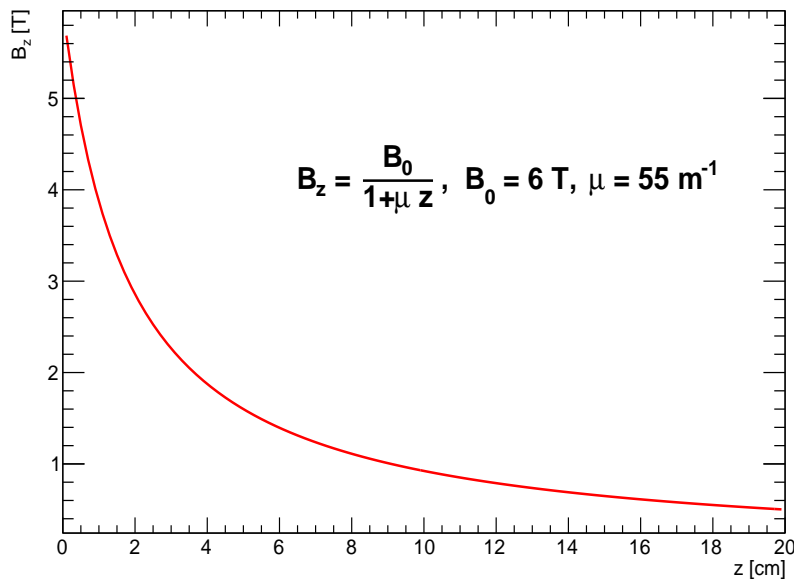

Figure 1: Demonstration of analytic AMD on-axis magnetic field, B_z, as a function of z.

provide a large energy acceptance and transform the positron phase spaces into larger transverse dimensions and smaller momentum spread which makes the beam easier to transport.

The pre-injector linac, made of many $2\,\mathrm{GHz}$ RF cativities, surrounded by a $0.5\,\mathrm{T}$ solenoid, has an inner aperture radius of $20\,\mathrm{mm}$. Positrons from the AMD are accelerated by the pre-injector linac to a designed energy of $200\,\mathrm{MeV}$. For this purpose, a long linac is used, composed of 11 Travelling Wave (TW) structures with a constant gradient at the $2\pi/3$ mode [10]. Each TW structure is supposed to be $1.5\,\mathrm{m}$ long and is composed of 30 accelerating cells. The distance between two TW structures is $20\,\mathrm{cm}$. The first TW structure works in decelerating mode to improve the capture of positrons, and the other structures work in accelerating mode to accelerate the positrons to $200\,\mathrm{MeV}$.

Finally a common e^+/e^- injector linac is used to accelerate both electrons and positrons from 200 MeV to 2.86 GeV. The optics design of the injector linac is aimed at the positrons, due to the fact that the emittance of the positron beam is much larger than the electron beam. The principle of the design is that the beam should be transported with as little loses as possible to the PDR. Earlier designs [11–14] require a bunch compressor after the pre-injector linac, so as to rotate the phase space and maximise the positron yield within the longitudinal acceptance of the PDR. But a recent study [15] in 2017 proposed to use several sections of FODO lattices instead. Consequently, after an optimisation of the pre-injector linac, the rotation of the phase space is no longer necessary. The aperture of the injector linac, which is the main limiting factor for the beam transport due to the large transverse emittance of the positron beam, is designed to be 20 mm (iris radius). The same accelerating structure with the same RF frequency as in the pre-injector linac is used.

The simulation of the CLIC positron source uses several different simulation tools. GEANT4 [16] is used to simulate the generation of primary electrons, the tungsten targets, the dipole between the targets and the transport and interactions with targets of particles, except for the channelling process of electrons in crystal tungsten, which is simulated by FOT [17] that is interfaced to GEANT4. Sampling with gaussian function is used to generate the four-momentum, transverse position and initial time for the primary electrons. The energy and momentum spread, spot size and beam length (divided by c, the speed of light in vacuum) are used as the standard deviation, σ, for the gaussian function. The AMD and the pre-injector linac are simulated by RF-TRACK [18]. The conical inner aperture of the AMD is also considered and simulated by using the latest version of RF-TRACK. Normally, the inner aperture radius of AMD is ranging linearly from $\sim$5.8 mm to 20 mm. But the inner aperture radius at the entrance can be changed in the optimisation, depending on the maximum magnetic field [19]:

$$R_1^2 = \frac{B_1}{B_2} \cdot R_2^2 , \tag{2}$$

where, R_1 is the inner aperture radius at the entrance, $B_1 = 6$ T is the maximum magnetic field, $B_2 = 0.5$ T is the minimum magnetic field, $R_2 = 20$ mm is the inner aperture radius at the exit. The simulation of the injector linac is actually extremely simplfied with an assumption that there are no losses of positrons in the injector linac, based on recent studies [10, 15]. A formula is used to calculate the positron energy at the end of the injector linac:

$$E_{\text{end}} = E_{\text{begin}} + (E_{\text{exp}}^{\text{PDR}} - E_{\text{ref}}) \cdot \cos(\omega \cdot (t - t_{\text{ref}})) , \tag{3}$$

where, E_{begin} and E_{end} are positron energies at the entrance and the exit of the injector linac, $E_{\text{exp}}^{\text{PDR}} = 2.86$ GeV is the designed energy that the positrons are expected to have at the end of the injector linac or the entrance of the PDR, $E_{\text{ref}} = 200$ MeV is the reference energy and is fixed to the designed energy at the end of the pre-injector linac, ω is the angular frequency corresponding to an RF frequency of 2 GHz, t is the time of positrons at the entrance of the injector linac and t_{ref} is the reference time.

The PDR is also not simulated, therefore, to calculate the effective positron yield, a time and energy window is used to select positrons that can be accepted by the PDR:

$$\begin{aligned} \Delta t_{e^+}^{\text{PDR}} &= 6\sigma_{\text{T}}^{e^+} \\ E_{e^+} &= E_{\text{exp}}^{\text{PDR}} \cdot (1 \pm \delta_E^{e^+}) , \end{aligned} \tag{4}$$

where, $\sigma_{\text{T}}^{e^+} = 3.3$ mm/c correspondes to a positron beam length of $\sigma_Z = 3.3$ mm at the entrance of the PDR, $E_{\text{exp}}^{\text{PDR}} = 2.86$ GeV is the designed energy at the entrance of the PDR, $\delta_E^{e^+} = 1.2\%$ correspondes to the positron momentum and energy acceptance of the PDR at the entrance.

The PEDD in the targets is also estimated using GEANT4. The mesh cells that are used to calculate PEDD have a constant volume, which is $\Delta x \cdot \Delta y \cdot \Delta z = 0.5\,\text{mm} \cdot 0.5\,\text{mm} \cdot 0.5\,\text{mm}$ in the three dimensional GEANT4 simulation coordinate system. The PEDD is always normalised to specific number of bunches per train and bunch population, therefore, the calculation of PEDD is expressed as:

$$\text{PEDD} = \frac{\max(E_{\text{dep}}^{\text{amor}})}{V_{\text{cell}} \cdot \rho_W \cdot n_{e^-}^{\text{sim}}} \cdot \frac{n_b \cdot n_{e^+}^{\text{PDR}}}{\eta_{e^+}^{\text{eff}}}, \tag{5}$$

where, $\max(E_{\text{dep}}^{\text{amor}})$ is the maximum deposited energy of all particles in a single mesh cell in the amorphous target [1], $V_{\text{cell}} = 0.125\,\text{mm}^3$ is the volume of a single mesh cell, $\rho_W = 19.3\,\text{g/cm}^3$ is the density of tungsten, $n_{e^-}^{\text{sim}} = 10^4$ is the number of simulated primary electrons, n_b is the number of bunches per train, $n_{e^+}^{\text{PDR}}$ is the target positron bunch population at the entrance of the PDR, $\eta_{e^+}^{\text{eff}}$ is the effective positron yield of positrons that are accepted by the PDR.

3 Validation of the simulation code

The validation of the CLIC positron source simulation code is performed by reproducing the ILC positron source (electron-driven) simulation results [20,21], since the design of the ILC positron source is quite similar as CLIC. Nevertheless, there are still some differences, for example, for the ILC positron source, the target is composed of a single rotating target with material being the tungsten rhenium (W-Re 26%) alloy; Standing Wave (SW) structures with L-band at 1.3 GHz are used in the pre-injector linac instead of TW structures; the injector linac is composed of a chicane, a booster linac and an energy compressor section (ECS), but the injector linac is also not simulated at ILC. Besides, different simulation tools are used, as summarised in Table 1.

Table 1: Simulation tools used for the ILC and CLIC positron sources.

Simulation tools	Target	AMD	SW or TW structures	Injector linac
ILC	GEANT4 or General Particle Tracker (GPT)	GEANT4	GEANT4	Analytic (not simulated)
CLIC	Fot and GEANT4	RF-TRACK	RF-TRACK	Analytic (not simulated)

For the input electron beam, the primary energy and beam size are 3 GeV and 2 mm, respectively. The acceptance of the damping ring (DR) that is located after the ILC injector linac is considered by applying a time window of $\pm 7\,\text{mm/c}$ on the time of positrons arriving at the SW structures exit. The target positron population at the entrance of the DR is $n_{e^+}^{\text{DR}} = 3^{10}$ (4.8 nC), while the number of bunches per train is supposed to be $n_b = 66$, and there is no overlap between the bunches given that the target is rotating at 225 rpm with 0.5 m diameter. As a result, the comparison of positron yield and PEDD is presented in Table 2.

A good agreement in the final accepted yield and PEDD with both differences less than 10% is observed between the ILC results and the reproduced results with the CLIC code [22]. Although the largest differences (10%-20%) are observed during the transport of the beam in the AMD and the SW structures, it is mainly due to particle interactions at the structure boundary which are considered in GEANT4 and not in RF-TRACK, and it does not affect much the final results and can be normally neglected.

---

[1]PEDD is usually only considered in amorphous target, since the PEDD in the crystal target is found to be relatively much smaller [1].

Table 2: Comparison of positron yield and PEDD between the ILC results and the reproduction with the CLIC code.

Positron yield	After target	After AMD	After the 1st SW structure	After all 36 SW structures	Accepted by DR	PEDD (2.4 nC e$^-$ bunch)
ILC results	7.13	5.09	2.58	1.94	**1.03**	**22.0**
Reproduction	7.07	4.48	2.03	1.97	**1.11**	**23.7**
Differences	1%	12%	21%	2%	**8**%	**8**%

4 The new optimisation strategy

For any optimisation with multiple parameters or subsystems such as positron source, it is always thought that a global study, in other words a start-to-end study, is the best choice. In a start-to-end optimisation, all parameters or subsystems are studied simultaneously instead of separately, which is more reasonable considering the correlations between the parameters. In a previous study [23], the start-to-end optimisation has already been applied to optimise the CLIC positron source, and meanwhile, the Nelder-Mead algorithm [24] was used to search for the optimal values of the parameters.

Similarly, such a start-to-end optimisation still applies to the new optimisation strategy. But instead of using the Nelder-Mead algorithm, we have developed a new method that is based on iterative parameter scanning and is much simpler and faster. The procedure of the optimisation strategy can be described in steps:

- First it is necessary to initialise the free parameters that need to be optimised, which is namely a starting point for the optimisation.

- Then a scan of all the free parameters with different values in proper ranges will be performed separately but simultaneously, for example, during the scan of a free parameter, the other free parameters are fixed to the starting point. As a result of the scan, for each free parameter, an optimised value is estimated by requiring a maximum positron yield and a PEDD that is as small as possible. This step is also called the first iteration of scan.

- Before performing the second iteration of scan, a new starting point is necessary and should be determined from the first iteration. This is normally achieved by simply taking the optimised values for all the free parameters that have been estimated in last step. However, due to the potential correlations between the free parameters, and to make sure that the iterations always give a better result, it is always necessary to compare the result from using all the optimised parameters, with the results from using a single optimised parameter. Parameters with values that give the best result in last iteration are always taken to be the new starting point for the next iteration.

- The iteration will be continued and the scan will be repeated, till the optimisation is finished and satisfied. Normally, after several iterations of scan, the free parameters and the results will become stable and can not be improved anymore, and the optimisation is thought to be finished.

Compared to the old optimisation strategy where the Nelder-Mead algorithm was used, the new optimisation strategy has the following advantages:

- Much simpler and faster. The idea of the new strategy is quite simple and easy to understand and implement. Normally, if the requirements on the free parameters are clear enough, the optimisation is found to be finished in a few iterations of scan, e.g. it usually takes 4 to 6 iterations. This is very fast, especially considering that the scan for each free parameter can be performed in parallel for

each iteration, and in principle if the computing resources are adequate, e.g. computer clusters where jobs can be divided and distributed by the HTCondor system or the IBM Platform LSF system, the optimisation time does not depend on the number of free parameters. Contrariwise, the old strategy performed the optimisation in a sequential manner, which therefore can not benefit much from the computing resources and relies on the number of free parameters.

- It is easy to find the global optimised results with the new optimisation method by looking at the scan plots. Contrariwise, it is easily to fall into a local minimum or maximum with the Nelder-Mead algorithm. An example would be the $f(x) = x \cdot \sin(x)$ function in a limited range, as demonstrated in Figure 2. The old optimisation algorithm always falls into the closest local peak or trough to the starting point, while the new strategy always finds the global maximum peak or minimum trough.

- The new optimisation strategy always gives the optimised parameters, since for each iteration of scan, the starting point is always required to be more optimised than last starting point. Contrariwise, the Nelder-Mead algorithm does not always converge, especially for non-mathematical parameter optimisations that are discontinuous or not very smooth.

- It is easy to control the new optimisation procedure. By looking at the scan plots, we do not have to use a decimal number as an optimised value. We can always use a integer or a rounded number, if it makes little difference, and that is very easy to know from the plots. Contrariwise, using the Nelder-Mead algorithm is like using a black box, which we can not control easily.

- The optimisation results of the new strategy are more convincing and reliable. Visual plots can be drawn for the scan results for each free parameter, from which it is easy to observe the tendency of how results are changed with the parameters. Such detailed and visible information can not be found if the Nelder-Mead algorithm is used. From the tendencies that have been observed, the optimised values of the free parameters are also quite flexible to be changed, tuned or rounded.

- The scan allows us to observe the individual effects from the free parameters and artificially control the optimisation process to go in the right direction that we wish. For instance, if the result does not change much when a parameter is changed around the optimised value, we can take a value that costs less, or sometimes make a compromise if a better result leads to a higher cost.

Even though the Nelder-Mead algorithm is a very popular method that is well designed for most mathmatical problems and provides very accurate results, in reality or for realistic parametric problems that are irregular and not smooth, the new optimisation strategy would be a better choice. To demonstrate how the strategy works, a practical example will be shown below to optimise the CLIC positron source with the new strategy.

In this example, the optimisation of the CLIC positron source is aimed at the 3 TeV and 1.5 TeV stages [2]. For the primary electron beam, to simplify the optimisation, the energy of the primary electron beam is fixed to $E_{e^-} = 5\,\text{GeV}$. However, we will anyway still perform a scan on the energy at the end of the optimisation, to see the impact of it on the results. The energy and momentum spread is fixed to be:

$$
\sigma_{E_{e^-}}/E_{e^-} = 0.1\%
$$
$$
\sigma_{p_x, p_y} = \frac{1}{\gamma_e} \cdot \frac{\varepsilon}{\sigma_{x,y}} \,,
\tag{6}
$$

---

[2] CLIC is assumed to be built and operated in a staged approach with three centre-of-mass energy stages: 380 GeV, 1.5 TeV and 3 TeV.
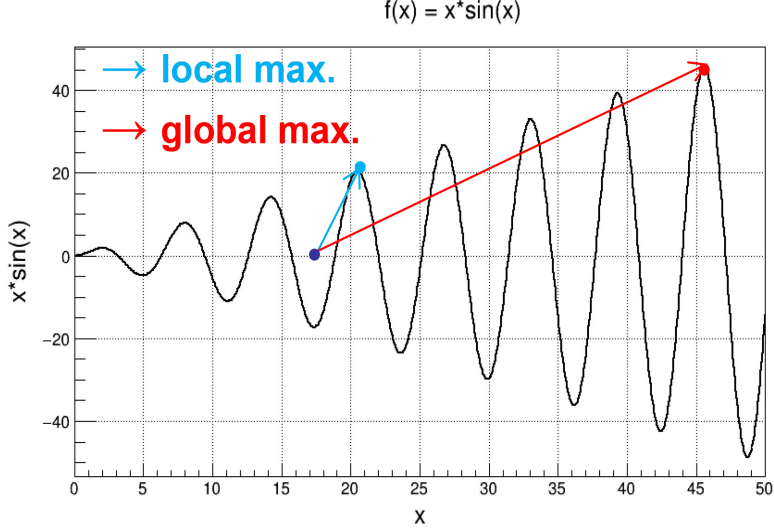
Figure 2: Demonstration of local fit and global fit with the $x \cdot \sin(x)$ function.

where, $\gamma_e = \frac{E_{e^-}}{m_0^e c^2}$ is the Lorentz factor of electron, ε is beam emittance, $\sigma_{x,y}$ is beam spot size. The initial time spread of the electron beam is taken to be $1\,\mathrm{mm/c}$, which corresponds to a beam length of $1\,\mathrm{mm}$. For the normalisation of PEDD, the number of bunches per train and the target positron bunch population at the entrance of the PDR are taken, respectively, to be $n_b = 312$ and $n_{e+}^{\mathrm{PDR}} = 4.44 \times 10^9$ (equal to 3.7×10^9 plus a 20% safe margin considered for the subsequent beam transport). The main parameters used in the simulation of the CLIC positron source including 12 free parameters for the optimisation are summarised in Table 3.

The starting point for the first iteration of scan is summarised in Table 4, where the free parameters are initialised arbitrarily. As a result, the effective positron yield is $0.87\,e^+/e^-$, and the corresponding PEDD (in amorphous target) is $36.2\,\mathrm{J/g}$.

Based on the starting point, a scan of all the 12 free parameters is performed simultaneously. But when we scan a parameter, the other parameters are fixed to the starting point. So the scan is also performed separately for each parameter. The scan results for the first iteration are presented in Figure 3. The effective positron yield and the PEDD (in amorphous target) are shown for the scan. To have a better display of the two quantities, the PEDD is scaled by $1/(35\,\mathrm{J/g})$.

The optimised values of the free parameters from the first iteration of scan, as well as the corresponding yield and PEDD values using a single optimised value or using all optimised values, are summarised in Table 5. Value of each parameter is obtained by requiring a positron yield that is as larger as possible, and a PEDD that is below $35\,\mathrm{J/g}$ and as smaller as possible. For most free parameters, it is not difficult to choose the optimised values, due to the fact that a higher yield usually gives a lower PEDD given that the other quantities in the definition of PEDD are not changed or changed not so much. But for parameters like the spot size of the electron beam, it is observed that a higher yield comes with a higher PEDD, due to the fact that a higher yield means a smaller spot size and a more focused beam. In that case, a compromise needs to be made between requiring a high yield and a low PEDD. The optimised values of free parameters for the first iteration of scan are decided based on the following reasons:

σ_{xy}: The optimised value of the e^- beam spot size is conservatively chosen to be $2.8\,\mathrm{mm}$, since it is obvious that when the spot size is larger than $2.8\,\mathrm{mm}$, the PEDD is almost not changed but the yield becomes

Table 3: Main parameters for 3 TeV (1.5 TeV) stage CLIC positron source simulation.

Parameters		Symbol	Units	Value
	Energy	E_{e^-}	GeV	5
	Spot size	σ_{xy}	mm	To be optimised
	Emittance	ε	mm·mrad	To be optimised
Primary e^- beam	Number of bunches per train	n_b		312
	Bunch spacing	Δt_b	ns	0.5
	Repetition frequency	f_{rep}	Hz	50
	Target bunch population	$n_{e^+}^{\text{PDR}}$	10^9	4.44
e^+ beam at the entrance of the PDR	Target energy	$E_{\text{exp}}^{\text{PDR}}$	GeV	2.86
	Effective energy acceptance	$\delta_E^{e^+}$	%	1.2
	Crystal target thickness	W_{crys}	mm	To be optimised
Hybrid target system	Amorphous target thickness	W_{amor}	mm	To be optimised
	Distance between two targets	D_{targ}	m	To be optimised
	Dipole magnetic field	B_{targ}	T	To be optimised
AMD	Maximum magnetic field	B_0	T	To be optimised
	Length	L_{amd}	cm	To be optimised
	Decelerating phase	ϕ_{dec}	degree	To be optimised
TW structures	Accelerating phase	ϕ_{acc}	degree	To be optimised
	Decelerating gradient	E_{dec}	MV/m	To be optimised
	Accelerating gradient	E_{acc}	MV/m	To be optimised

Table 4: Starting point of free parameters for the first iteration of scan. Parameters are defined in Table 3.

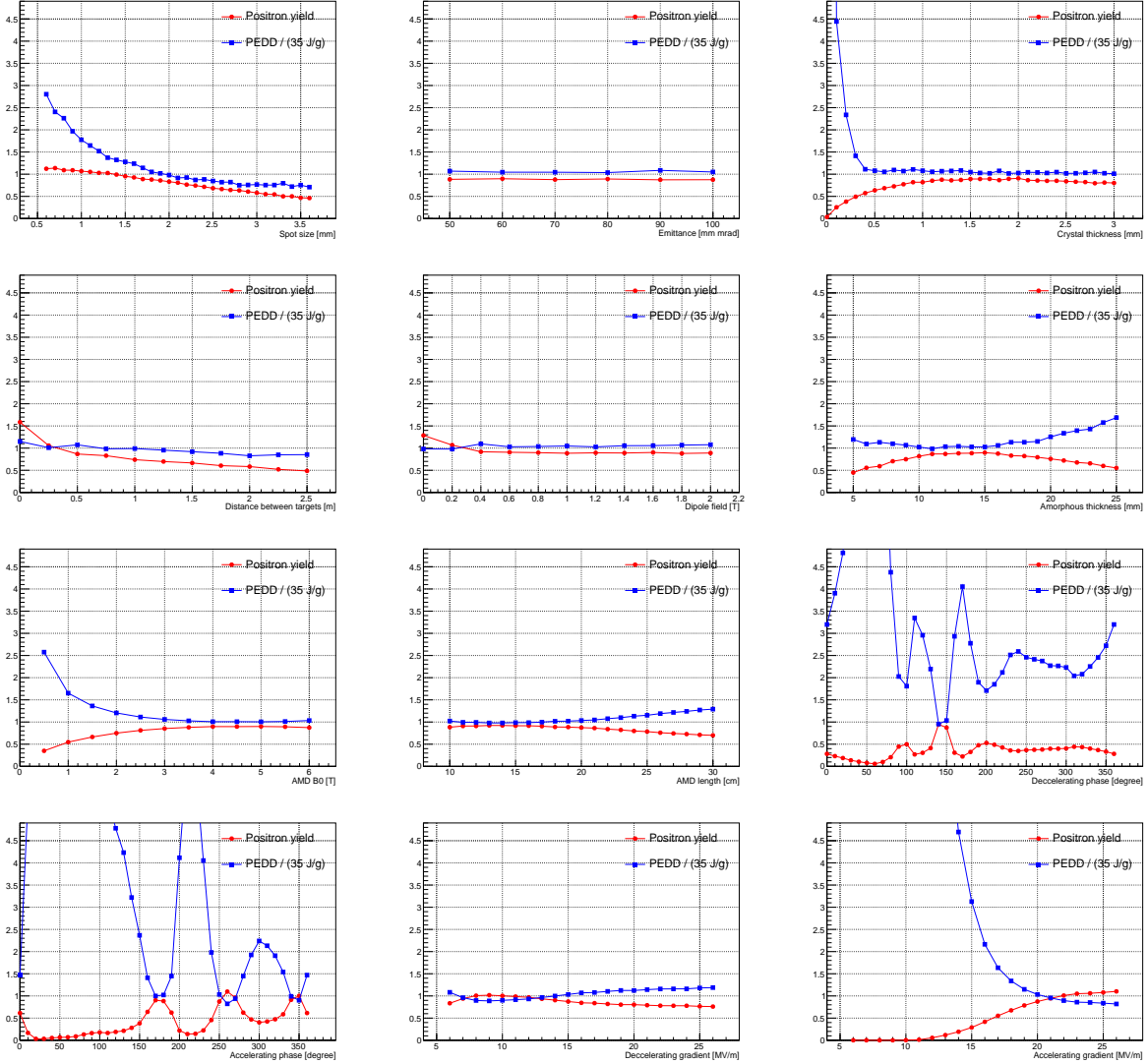| σ_{xy}	ε	W_{crys}	W_{amor}	D_{targ}	B_{targ}	B_0	L_{amd}	ϕ_{dec}	ϕ_{acc}	E_{dec}	E_{acc}	$\eta_{e^+}^{\text{eff}}$	PEDD
1.8 mm	80 mm·mrad	1.5 mm	15 mm	0.5 m	1 T	6 T	20 cm	150°	250°	15 MV/m	20 MV/m	0.87 e^+/e^-	36.2 J/g

Figure 3: Scan results of the first iteration for the 12 free parameters. The optimised values for the free parameters are summarised in Table 5.

smaller and smaller.

ε: The positron yield and PEDD are found to be independent on the e^- beam emittance, thus the optimised value is the same with the initial value, 80 mm·mrad, which is also thought to be a reasonable value.

$W_{\mathbf{crys}}$: The optimised value of the crystal target thickness is chosen to be 1.5 mm, due to the same consideration as σ_{xy}.

$W_{\mathbf{amor}}$: The optimised value of the amorphous target thickness is chosen to be 15 mm, since the yield is maximum and the PEDD is minimum.

$D_{\mathbf{targ}}$: The optimised value of the distance between the two targets is chosen to be 0, since the yield is maximum and the gain in yield is obvious. Though the PEDD is not minimum and exceeds the 35 J/g limit, we can always decrease the PEDD by further optimising other parameters and increasing the

yield.

$B_{\mathbf{targ}}$: The optimised value of the magnetic field of the dipole between the targets is also found to be 0, with a maximum yield and a minimum PEDD.

B_0: The optimised value of the AMD maxmimum magnetic field is chosen to be 4 T, which is the minimum value that achieves a maximum yield and a minimum PEDD.

$L_{\mathbf{amd}}$: The optimised value of the length of the AMD is chosen to be 15 cm, with a maximum yield and a minimum PEDD.

$\phi_{\mathbf{dec}}$: The optimised value of the TW deceleraing phase is found to be 140°, with a maximum yield and a minimum PEDD.

$\phi_{\mathbf{acc}}$: The optimised value of the TW accelerating phase is found to be 260°, with a maximum yield and a minimum PEDD.

$E_{\mathbf{dec}}$: The optimised value of the TW deceleraing gradient is chosen to be 10 MV/m, with a maximum yield and a minimum PEDD.

$E_{\mathbf{acc}}$: The optimised value of the TW acceleratnig gradient is chosen to be 26 MV/m, with a maximum yield and a minimum PEDD.

For some of the free parameters, the optimised values might be chosen too conservative or not the optimal, but it is not a big problem, since the optimisation is based on iterations of scan. Choosing the optimised values for free parameter properly is important and would reduce the optimisation time, but the optimal results depend only on the final iteration.

Table 5: Optimised values of free parameters from the first iteration of scan. Parameters are defined in Table 3. Positron yield and PEDD are also presented using a single optimised value (the last two rows) or using all optimised values (the last column).

Free parameters	σ_{xy}	ε	W_{crys}	W_{amor}	D_{targ}	B_{targ}	B_0	L_{amd}	ϕ_{dec}	ϕ_{acc}	E_{dec}	E_{acc}	All used
Optimised value	**2.8 mm**	80 mm·mrad	1.5 mm	15 mm	**0**	**0**	**4 T**	**15 cm**	**140°**	**260°**	**10 MV/m**	**26 MV/m**	
$\eta_{e^+}^{\mathrm{eff}}$ $[e^+/e^-]$	0.63	0.89	0.89	0.90	**1.59**	1.29	0.90	0.92	0.95	1.10	1.00	1.10	**0.54**
PEDD [J/g]	26.3	36.3	36.7	35.9	**40.2**	34.3	35.2	34.5	33.4	28.8	31.5	28.7	**56.8**

The effective positron yield and PEDD are found to be $0.54\,e^+/e^-$ and 56.8 J/g when all the optimised parameters are used, which are worse than most results when only a single optimised parameter is used. The highest yield is achieved at $1.59\,e^+/e^-$ when the distance between targets is 0, but the corresponding PEDD is 40.2 J/g, which is larger than the 35 J/g limit. To reduce the PEDD, it is necessary to increase the e^- beam spot size, though the yield will also be decreased. Therefore, finally only two optimised values are used: $\sigma_{xy} = 2.8$ mm and $D_{\mathrm{targ}} = 0$. Since the distance between targets is 0, the dipole is not needed any more: $B_{\mathrm{targ}} = 0$. As a result, the starting point for the second iteration of scan can be fixed and are summarised in Table 6.

The scan results for the second iteration are presented in Figure 4. Due to the performance of the free parameters in the first iteration, the scan for ε, D_{targ} and B_{targ} is thought to be not necessary and is thus not performed. Therefore, only 9 free parameters are scanned in the second iteration.

Table 6: Starting point of free parameters for the second iteration of scan. Parameters are defined in Table 3.

σ_{xy}	ε	W_{crys}	W_{amor}	D_{targ}	B_{targ}	B_0	L_{amd}	ϕ_{dec}	ϕ_{acc}	E_{dec}	E_{acc}	$\eta_{e^+}^{\text{eff}}$	PEDD
2.8 mm	80 mm·mrad	1.5 mm	15 mm	**0**	0	6 T	20 cm	150°	250°	15 MV/m	20 MV/m	**1.09** e^+/e^-	**28.7 J/g**
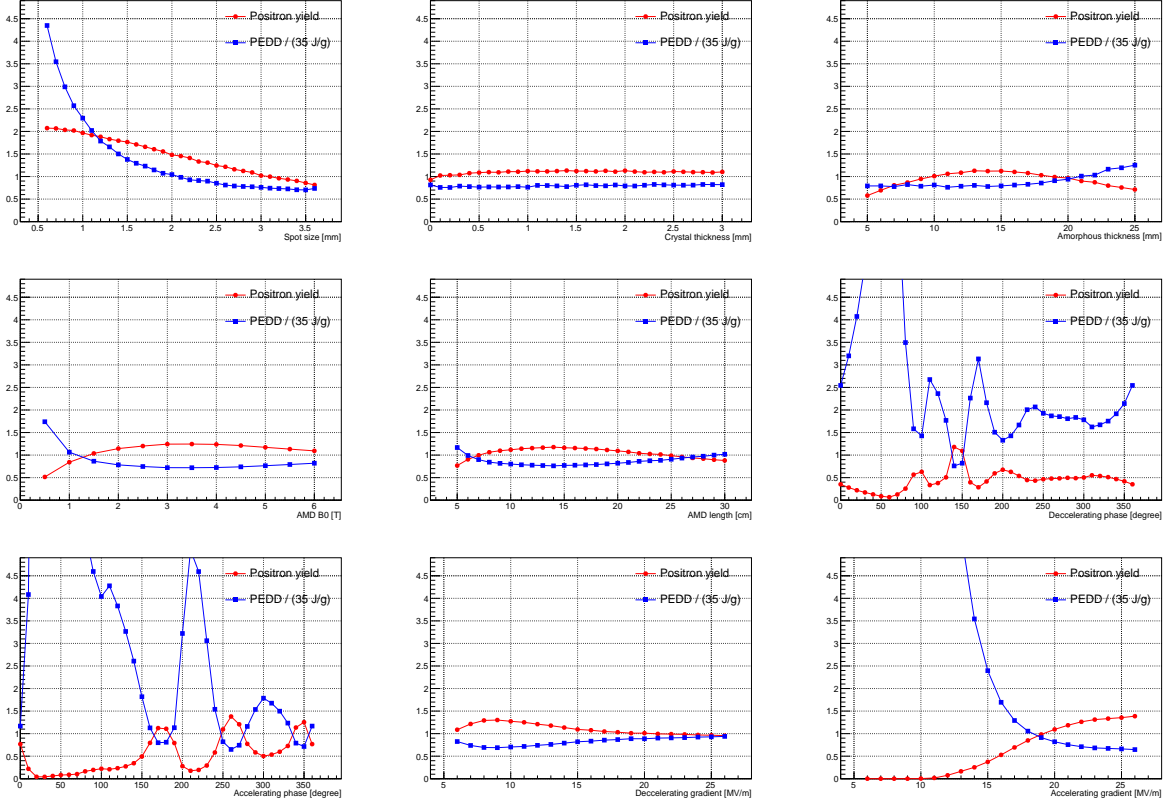
Figure 4: Scan results of the second iteration for the free parameters.

The optimised values for the free parameters for the second iteration are chosen, and the starting point for the third iteration is selected, in a similar way as what we did in the first iteration. The iterations are continued by requiring a maximum effective positron yield, with a PEDD that is below 35 J/g and as small as possible, and that the optimised values for the free parameters should be as more realistic and economic as possible. Finally, after 6 iterations of scan, the final optimised results are obtained, as presented in Table 7;

Table 7: Final optimised results. Parameters are defined in Table 3.

σ_{xy}	ε	W_{crys}	W_{amor}	D_{targ}	B_{targ}	B_0	L_{amd}	ϕ_{dec}	ϕ_{acc}	E_{dec}	E_{acc}	$\eta_{e^+}^{\text{eff}}$	PEDD
1.7 mm	**80 mm·mrad**	**1 mm**	**14 mm**	**0**	**0**	**6 T**	**18 cm**	**150°**	**260°**	**10 MV/m**	**19 MV/m**	**2.22** e^+/e^-	**31.2 J/g**

Nevertheless, a final scan is performed for the optimised parameters, as shown in Figure 5. It is obvious that the optimised results are stable and optimal, which fulfills the requirement that the optimisation is finished.

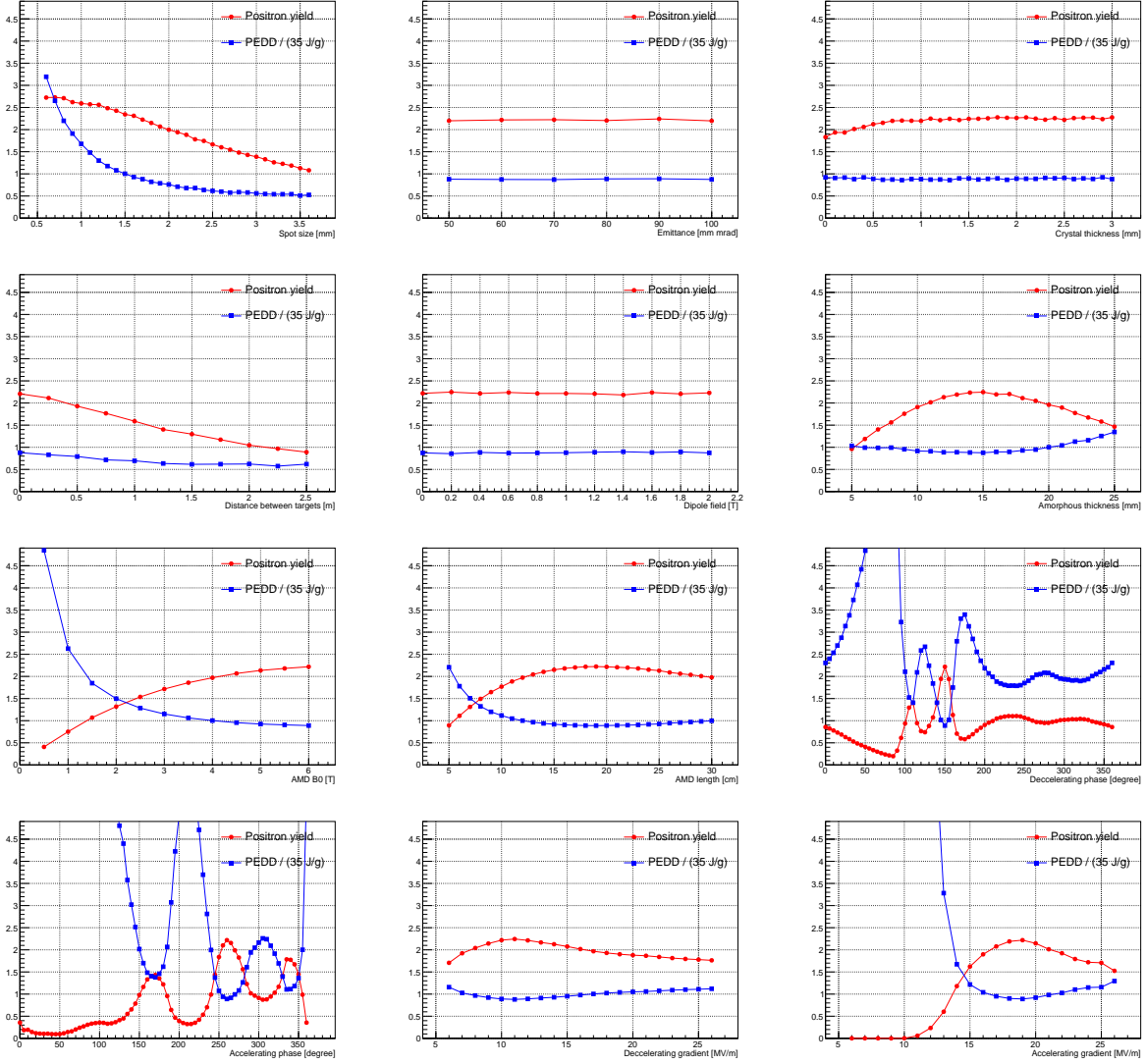As a result of using the final optimised positron source parameters obtained above, the phase spaces of

Figure 5: Final scan results for the free parameters.

the positron beam at the exit of the first TW structure and the end of the pre-injector linac are presented in Figures 6 and 7, respectively.
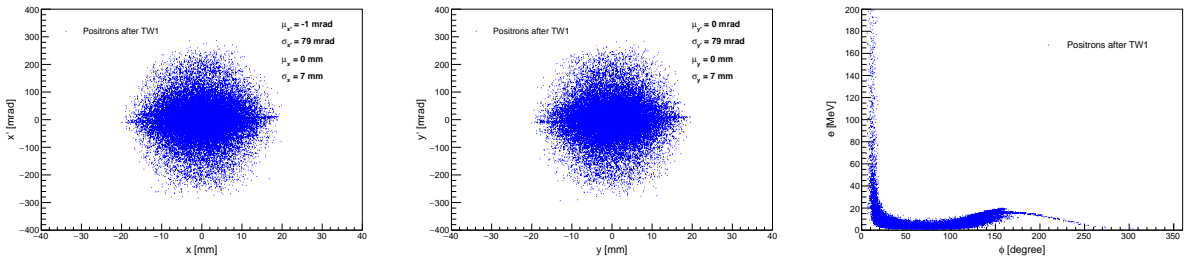

Figure 6: Phase spaces of the positron beam at the exit of the first TW structure.

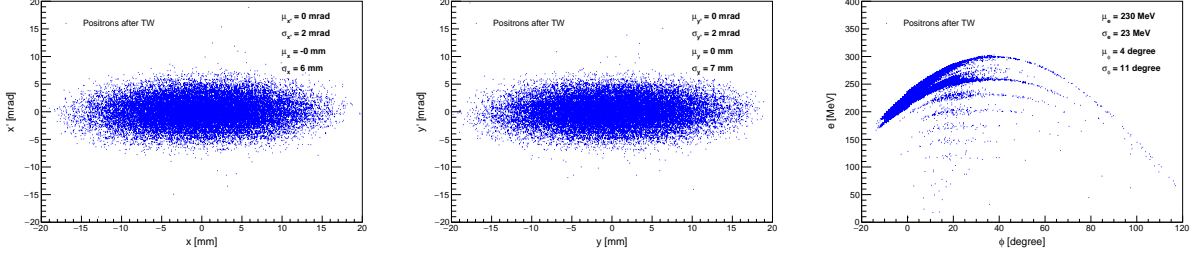The energy distributions of the positrons at the exit of the target, AMD and pre-injector are also compared

13

Figure 7: Phase spaces of the positron beam at the exit of the first TW structure.

and presented in Figure 8 in the left plot. While in the right plot, the energy distribution at the exit of the injector linac is presented, with the red dashed lines marking the 1.2% accepted energy window around 2.86 GeV by the PDR.
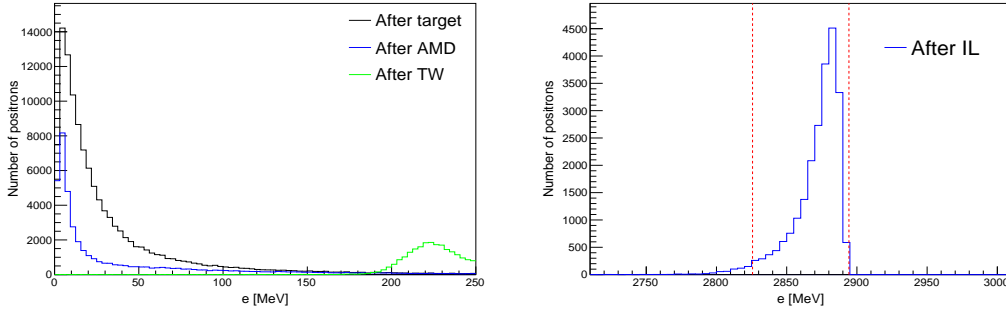

Figure 8: Energy distributions at the exit of different sections of the positron source. The red dashed lines in the right plot shows the accepted energy window by the PDR.

Besides, an additional scan of the e^- primary energy, E_{e^-} based on the optimised free parameters, is performed to see the possibility to change the e^- energy, as presented in Figure 9. The yield is observed to be increased with E_{e^-} almost linearly, while the PEDD is not much affected. This shows a possibility to further increase the yield without changing the PEDD by increasing the e^- primary energy, or a possibility to reduce the energy by sacrificing the yield, approximately in a linear way (e.g. $\eta_{e^+}^{\text{eff}} \approx 0.2 + 0.4 \cdot (E_{e^-}/\text{GeV})e^+/e^-$, when $3\,\text{GeV} < E_{e^-} < 5\,\text{GeV}$).

A big difference between the old parameters before the optimisation and the parameters after the optimisation is that, the dipole between the crystal and amorphous targets is removed. Although the dipole helps to reduce the energy deposition in the amorphous target by diverting the charged particles, the beam size is enlarged at the same time. The normalised PEDD can be also reduced by improving the final yield, which allows to completely remove the dipole and the distance between the two targets. However, further studies shows that it is also possible to remove the crystal target, with a small loss ($\leq 8\%$) in the final yield, as long as the total length of the target is not changed much (in this case, it should be around $1 + 14 = 15\,\text{mm}$).
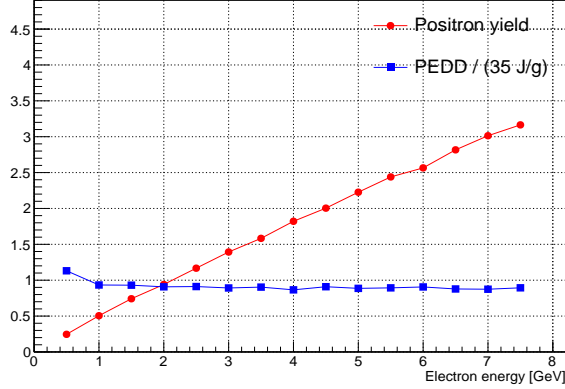
Figure 9: Additional scan of e^- primary energy based on the optimised free parameters. The default value is $5\,\mathrm{GeV}$.

5   Comparison with previous optimisation

In previous optimisation [23], the Nelder-Mead algorithm was used by calling the FMINSEARCH function in the GNU Octave software. The corresponding optimised positron yield for $5\,\mathrm{GeV}$ primary e^- is $1.94\,e^+/e^-$. However, in previous studies, the AMD was actually simulated with a constant inner aperture (20 mm radius) instead of a conical aperture that it is supposed to be, which would overestimate the positron yield by at least 25%. Taking this AMD correction into account, the previous positron yield will be about $1.55\,e^+/e^-$. Therefore, the new optimised positron yield is found to have an improvement of 43%, which is mainly due to that the constraint on the distance between the two targets is removed in the new optimisation, while in the previous optimisation, it was required to be larger than $0.5\,\mathrm{m}$. However, to make a fair comparison, we performed four tests to compare the new optimisation strategy with the Nelder-Mead algorithm.

In the first test, we performed an optimisation using the Nelder-Mead algorithm, in the same way that it was used in previous studies (the positron yield is set to be 0, if PEDD is found to be larger than the $35\,\mathrm{J/g}$ limit). Besides, the same parameters, starting point and contraints as that used in the new optimisation in Table 4 were used. As a result, the optimisation could not converge, mainly due to that the PEDD of the starting point is larger than the $35\,\mathrm{J/g}$ limit, and the Nelder-Mead algorithm is not able to handle such a situation.

Despite such a disadvantage, we anyway performed the second test, in which we used another starting point that gives a PEDD less than the $35\,\mathrm{J/g}$ limit, by simply changing the TW accelerating phase ϕ_{acc} from $250°$ to $260°$. As a result, the optimisation fell into a local maximum of positron yield, which is $1.18\,e^+/e^-$. The optimised results are summarised in Table 8.

Table 8: Optimised results of Nelder-Mead algorithm in the second test. Parameters are defined in Table 3.

σ_{xy}	ε	W_{crys}	W_{amor}	D_{targ}	B_{targ}	B_0	L_{amd}	ϕ_{dec}	ϕ_{acc}	E_{dec}	E_{acc}	$\eta_{e^+}^{\mathrm{eff}}$	PEDD
$1.81\,\mathrm{mm}$	$81.50\,\mathrm{mm\cdot mrad}$	$1.53\,\mathrm{mm}$	$15.26\,\mathrm{mm}$	0.504	1.02	$6.00\,\mathrm{T}$	$20.33\,\mathrm{cm}$	$154.67°$	$269.07°$	$15.24\,\mathrm{MV/m}$	$20.21\,\mathrm{MV/m}$	$1.18\,e^+/e^-$	$26.54\,\mathrm{J/g}$

Despite the failure and disadvantage of the Nelder-Mead algorithm in the second test, we perfomed the optimisation with another starting point which we think is already quite close to the new optimisation results and is already quite optimised. The new starting point for the optimisation in the third test is summarised in Table 9.

15

Table 9: Starting point for Nelder-Mead optimisation in the third test. Parameters are defined in Table 3.

σ_{xy}	ε	W_{crys}	W_{amor}	D_{targ}	B_{targ}	B_0	L_{amd}	ϕ_{dec}	ϕ_{acc}	E_{dec}	E_{acc}	$\eta_{e^+}^{\mathrm{eff}}$	PEDD
2.5 mm	80 mm·mrad	1.5 mm	15 mm	0.1	0.1	6 T	20 cm	150°	260°	15 MV/m	20 MV/m	1.51 e^+/e^-	23.85 J/g

As a result, the optimisation fell into a local maxmimum again, and did not give the optimal results as expected. The optimised results are summarised in Table 10.

Table 10: Optimised results of Nelder-Mead algorithm in the third test. Parameters are defined in Table 3.

σ_{xy}	ε	W_{crys}	W_{amor}	D_{targ}	B_{targ}	B_0	L_{amd}	ϕ_{dec}	ϕ_{acc}	E_{dec}	E_{acc}	$\eta_{e^+}^{\mathrm{eff}}$	PEDD
2.56 mm	80.52 mm·mrad	1.52 mm	15.26 mm	0.10	0.10	6.00 T	20.20 cm	153.97°	265.49°	15.25 MV/m	20.50 MV/m	1.53 e^+/e^-	22.00 J/g

In the fourth test, we removed the 35 J/g limit on PEDD in the optimisation. In this case, the Nelder-Mead algorithm is supposed to be able to converge. Therefore, the same starting point as that used in the first test was used. As a result, the optimisation fell into a local maxmimum again. Besides, the optimised PEDD is 34.46 J/g, which is thought to be not safe enough, though it is smaller than the 35 J/g limit. The optimised results are summarised in Table 11.

Table 11: Optimised results of Nelder-Mead algorithm in the fourth test. Parameters are defined in Table 3.

σ_{xy}	ε	W_{crys}	W_{amor}	D_{targ}	B_{targ}	B_0	L_{amd}	ϕ_{dec}	ϕ_{acc}	E_{dec}	E_{acc}	$\eta_{e^+}^{\mathrm{eff}}$	PEDD
1.33 mm	88.67 mm·mrad	1.65 mm	13.68 mm	0.52	1.31	6.00 T	20.56 cm	160.33°	272.04°	13.21 MV/m	21.85 MV/m	1.35 e^+/e^-	34.46 J/g

It is possible for the Nelder-Mead algorithm to achieve a better result by repeating the optimisations for a few more times, with the starting point reset every time the optimisation is repeated. However, correspondingly, the total optimisation time would also be increased linearly.

For the optimisations above with the Nelder-Mead algorithm, the average number of evaluations or simulations of the positron source is about 300 times for each test without repetitions. If the time for one evaluation is ΔT, the total optimisation time will be $300 \cdot \Delta T$. But for the new optimisation, in principle, 6 iterations take only $6 \cdot \Delta T$, due to the fact that jobs can be run in parallel. Taking also the evaluation of the starting point for each iteration into account, the total optimisation time will be $12 \cdot \Delta T$. It means that the new optimisation strategy is 25 times faster than the old algorithm without repetitions. While with repetitions, the new optimisation strategy could be $25 \times N_{\mathrm{rep}}$ times faster than the old algorithm, where N_{rep} is the number of repetitions for the old algorithm to achieve the best result.

6   Study on mesh grid size for energy deposition in PEDD estimation

To reduce the impact on the PEDD estimation from the mesh grid size which is used in the target simulation by GEANT4 for the energy deposition purpose, it is necessary to make sure that the grid size is properly selected such that the uncertainty of the PEDD estimation is as lower as possible.

With the optimised beam and target parameters as shown in Table 7, PEDD can be dispersedly calculated in each single cell of the mesh grid. For a simplified and fair comparison, PEDD is always normalised to a given yield of $2.0\,e^+/e^-$ for all the cases. Therefore the PEDD distributions along the X, Y and Z coordinates at

peak energy deposition density position can be plotted and are presented in Figure 10. Statistical uncertainty on the distributed PEDD in the plots is taken to be $\sqrt{\sum pedd^2}$, where $pedd$ is calculated for each particle deposited in each single mesh cell. Double gaussian function and quadratic function are found to be the best fit functions for the transverse and longitudinal distributions, respectively, for most cases. The fit functions are expressed as follows:

$$f(x) = \alpha e^{\frac{(x-\mu)^2}{2\sigma_1^2}} + \beta e^{\frac{(x-\mu)^2}{2\sigma_2^2}}$$

$$f(y) = \alpha e^{\frac{(y-\mu)^2}{2\sigma_1^2}} + \beta e^{\frac{(y-\mu)^2}{2\sigma_2^2}} \tag{7}$$

$$f(z) = \lambda(z-\mu)^2 + \alpha$$

where, the functions reach the maximum at $x, y, z = \mu$, that is $\alpha + \beta$ for $f(x)$ or $f(y)$ or α for $f(z)$.
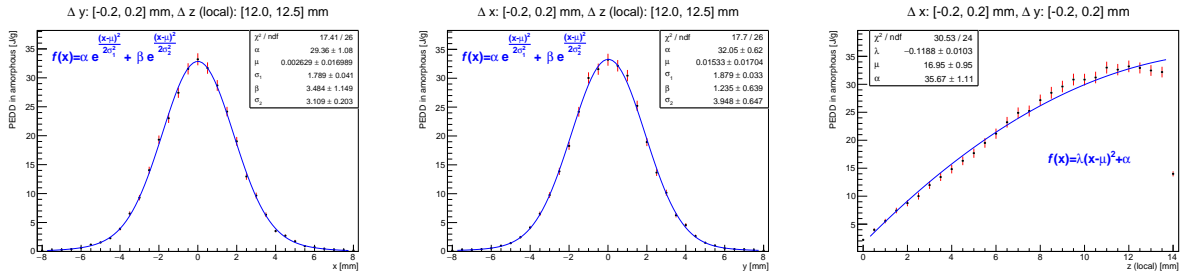
Figure 10: PEDD distributions along the X, Y and Z coordinates at peak energy deposition density position. PEDD normalised to a given yield of $2.0\,e^+/e^-$.

Obviously, we can see that the fits are very good, and there is very small difference (1%) between the peak of the distributed PEDD and the peak of the fit function. It confirms that the present mesh grid size $\Delta x \cdot \Delta y \cdot \Delta z = 0.5\,\text{mm} \cdot 0.5\,\text{mm} \cdot 0.5\,\text{mm}$ that is used in this report is very properly selected.

However, as an extension of the PEDD study and to prove that the 0.5 mm cubic mesh grid applies to most cases when the beam spot size is changed, it is necessary to perform a scan of the beam spot size, as well as a scan of the grid size. To simplify the study, the mesh grid is always required to be cubic, which means that the grid size is always equal along the X, Y and Z coordinates. The scanned values of the spot size are: 1.0 mm, 1.7 mm, 2.5 mm, 4.0 mm, 5.0 mm. The scanned values of the grid size are: 0.02 mm to 0.1 mm every 0.01 mm, 0.1 mm to 1.0 mm every 0.1 mm, 1.0 mm to 2.5 mm every 0.5 mm, and 5.0 mm.

As a result, there are totally 110 cases with different beam spot sizes or mesh grid sizes. For each case, the PEDD distributions are fitted with the functions mentioned above along the X, Y and Z coordinates. All the fitting details are not presented in this report, but the fitting results are summarised and presented in Figure 11. Comparison plots are drawn along the X, Y and Z coordinates from the left to the right, respectively, for each scanned spot size. In each plot, comparison of the raw PEDD [3] values and the fitted PEDD values is presented in the upper pad for different scanned cubic mesh grid sizes, while in the lower pad, ratios of the two PEDD values are calculated, as well as the the goodness of fit. The accepted grid sizes should always give a fitted to raw PEDD ratio that is not far from 1.0. In this study, the difference between the raw PEDD and the fitted PEDD is required to be no larger than 10%. As a consequence, the accepted grid size range can be estimated for each spot size, as summarised in Table 12. The estimation of the accepted grid size ranges is mainly based on the fit along the X and Y coordinates, since the fit goodness is much better than the fit along the Z coordinate.

---

[3]Raw PEDD refers to the PEDD calculated directly from maximum deposited energy instead of from fit, while fitted PEDD
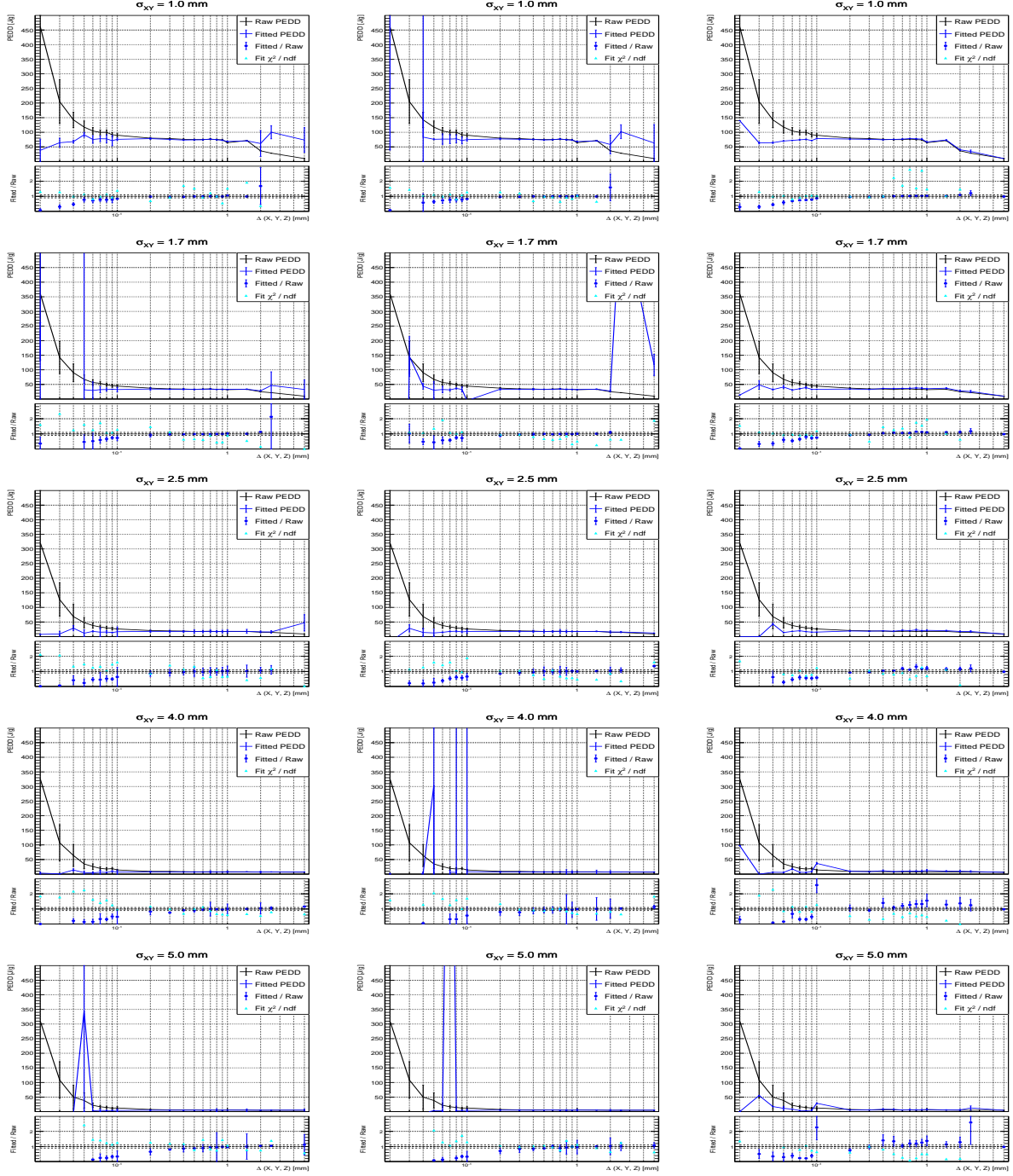
Figure 11: Comparison of PEDD distribution fit results along the X (left), Y (middle) and Z (right) coordinates at peak energy deposition density position for different scanned beam spot sizes and cubic mesh grid sizes. PEDD normalised to a given yield of $2.0\,e^{+}/e^{-}$.

The estimated accepted grid size ranges can be further drawn and fitted with linear functions for an extrapolation to a general case, as presented in Figure 12. Therefore, the accepted grid size range can be

refers to the PEDD from fit which is equal to the peak of the fit function.

Table 12: Accepted grid size ranges estimated from the fit for each scanned beam spot size.

Beam spot size [mm]	1.0	1.7	2.5	4.0	5.0
Accepted grid size range [mm]	[0.2, 1.5]	[0.2, 2.0]	[0.2, 2.5]	[0.4, 2.5]	[0.5, 5.0]

expressed by:

$$0.07 + 0.08 \cdot \sigma_{x,y} \leq \Delta(X, Y, Z) \leq 0.65 + 0.72 \cdot \sigma_{x,y} \tag{8}$$

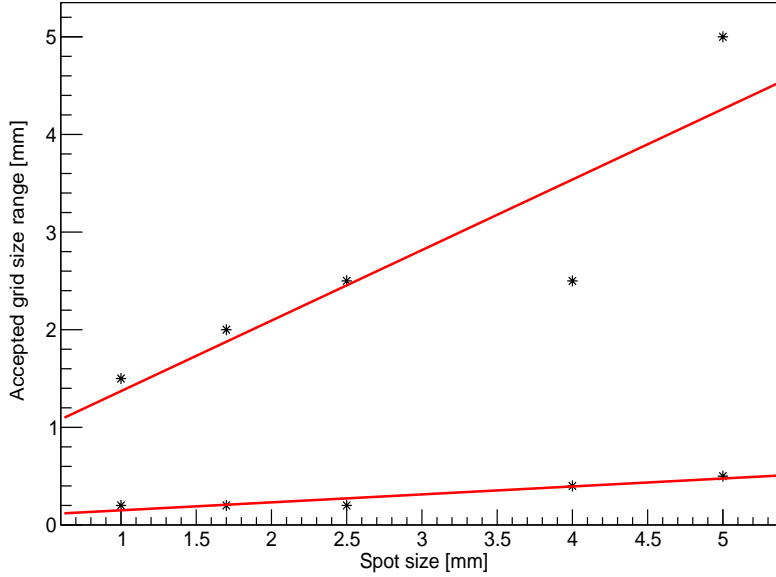where, $\Delta(X, Y, Z)$ is the cubic mesh grid size and $\sigma_{x,y}$ is the beam spot size. Units are millimeters.

Figure 12: Fit accepted grid size ranges with linear functions.

However, the study is performed with 10^4 simulated primary electrons at $5\,\text{GeV}$. To extrapolate to a general application of the study, it is necessary to do some scalings. According to the Freedman-Diaconis rule [25], which is developed and used to select the width of the bins to be used in a histogram in statistics, the suggested bin width of a distribution is:

$$\text{Bin width} = 2\frac{\text{IQR}(x)}{\sqrt[3]{n}} \tag{9}$$

where, $\text{IQR}(x)$ is the interquartile range of the data, and n is the number of observations in the sample x. In our case, n is the number of deposited particles along the X or Y coordinate, which is supposed to be varied proportionately to the variety of the number of simulated primary electrons, while $\text{IQR}(x)$ is thought to be not relevant to the number of primary electrons. Therefore, the scaling factor of the accepted mesh grid size due to the number of simulated primary electrons is:

$$\text{Scaling factor} = \sqrt[3]{\frac{10^4}{N_e}} \tag{10}$$

19

where, N_e is the number of simulated primary electrons.

The scaling of the mesh grid size due to the primary electron energy is also studied. Based on the scan of the primary electron energy as mentioned in Section 4, it is found that $\mathrm{IQR}(x)$ is not affected by the primary electron energy, for example, the value of $\mathrm{IQR}(x)$ is found to be constantly $1.5\,\mathrm{mm}$ along the X and Y coordinates. While n, the number of deposited particles along the X and Y coordinates, is found to be varied as a quadratic function of the primary electron energy as follows:

$$n_{x,y} \approx -500 \cdot E_{e^-}^2 + 9500 \cdot E_{e^-} + 5000 \tag{11}$$

where, E_{e^-} is the primary electron energy in GeV. Therefore, the scaling factor of the accepted mesh grid size due to the primary electron energy is:

$$
\begin{aligned}
\text{Scaling factor} &= \sqrt[3]{\frac{-500 \cdot 5^2 + 9500 \cdot 5 + 5000}{-500 \cdot E_{e^-}^2 + 9500 \cdot E_{e^-} + 5000}} \\
&= \sqrt[3]{\frac{80}{-E_{e^-}^2 + 19 \cdot E_{e^-} + 10}}
\end{aligned} \tag{12}
$$

where, E_{e^-} is the primary electron energy in GeV.

To summarise, the estimated accepted grid size range, with number and energy scaling factors of the primary electrons included, can be generally expressed as follows:

$$(0.07+0.08 \cdot \sigma_{x,y}) \cdot \sqrt[3]{\frac{10^4}{N_e}} \cdot \sqrt[3]{\frac{80}{-E_{e^-}^2 + 19 \cdot E_{e^-} + 10}} \leq \Delta(X,Y,Z) \leq (0.65+0.72 \cdot \sigma_{x,y}) \cdot \sqrt[3]{\frac{10^4}{N_e}} \cdot \sqrt[3]{\frac{80}{-E_{e^-}^2 + 19 \cdot E_{e^-} + 10}} \tag{13}$$

where, $\Delta(X,Y,Z)$ is the cubic mesh grid size and $\sigma_{x,y}$ is the beam spot size, with units both in millimeter. N_e is the number of simulated primary electrons and E_{e^-} is the primary electron energy in GeV.

It should be noticed that the scaling factors are always evaluated from the X and Y coordinates, due to the fact that the mesh is cubic in this study, and the energy deposition is thought to be symmetric in the transverse plane. While the energy deposition along the Z coordinate is thought to be not complete due to the limited length of the target, which nevertheless affect the estimation of the number of deposited particles. This is also one of the reasons for that the PEDD fit goodness along the X and Y coordinates is better than the Z coordinate.

7 Simulation of the injector linac

So far in this report, to simplify the optimisation, the injector linac is not actually simulated. A fast calculation of the positron energy is used instead, as already mentioned in Section 2. This is also based on the assumption that there are no losses of positrons in the injector linac, according to a recent study [15], which improved the design of the injector linac. Therefore, to simulate the injector linac, the same design is used in this report. PLACET [26] is used in simulation.

In order to make it work, the output positron beam from the pre-injector linac needs to be matched well to the injector linac design. A matching section is therefore put in front of the injector linac, composed of four quadrupoles. However, using the final optimised positron source parameters obtained in Table 7, it is quite difficult to match to existed design. This is due to that the mean energy of the positron beam at the

exit of the pre-injector linac is around 230 MeV, which is quite different from the designed energy at the entrance of the injector linac, which is around 200 MeV, and the energy spread, which is around 10%, is a bit higher than expected.

Therefore, the positron source is re-optimised again with the mean energy and energy spread at the end of the pre-injector linac included, aiming at a mean energy close to 200 MeV and an energy spread as low as possible, but without losing much yield. The optimisation plots of the final iteration of scan are presented in Figure 13. The final optimised parameters are summarised in Table 13 In addition to the effective positron yield and the PEDD (in amorphous target), the mean energy and energy spread of the positron beam at the end of the pre-injector linac are also displayed for the scan. To have a better display, the mean energy is scaled by 200 MeV and the energy spread is scaled by 3%.
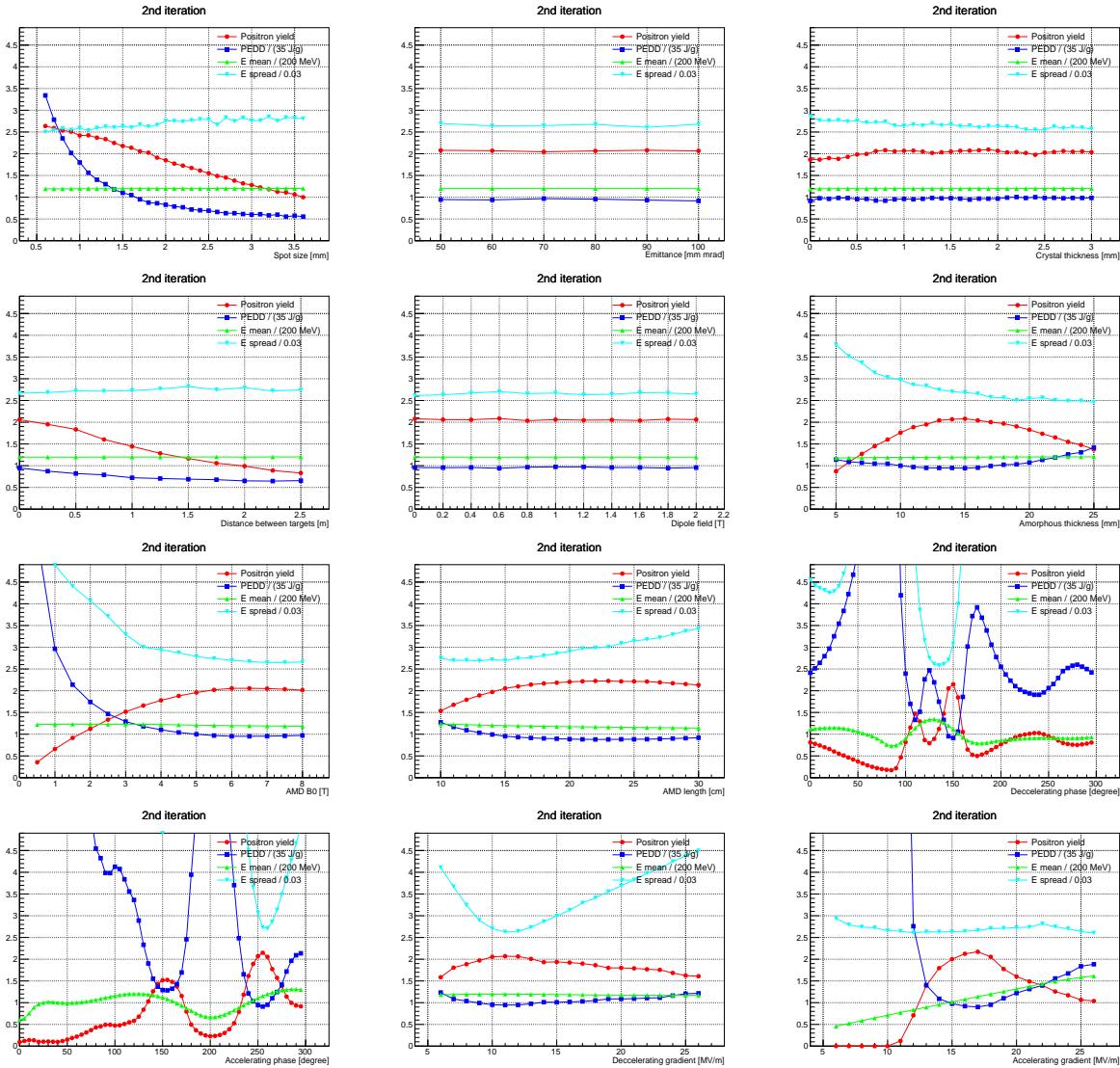

Figure 13: Final scan results for the free parameters of the re-optimisation for the injector linac matching.

After the re-optimisation, the mean energy of the positron beam at the exit of the pre-injector linac is reduced to ~204 MeV, and the energy spread is reduced to ~ 7%. With a separate optimisation of the matching section and the initial reference energy of the injector linac, the positron beam can now be well

Table 13: Final optimised results of the re-optimisation for the injector linac matching. Parameters are defined in Table 3.

σ_{xy}	ε	W_{crys}	W_{amor}	D_{targ}	B_{targ}	B_0	L_{amd}	ϕ_{dec}	ϕ_{acc}	E_{dec}	E_{acc}	$\eta_{e^+}^{\text{eff}}$	PEDD
1.7 mm	80 mm·mrad	1 mm	15 mm	0	0	6 T	15 cm	145°	260°	10 MV/m	15 MV/m	2.00 e^+/e^-	34.1 J/g

matched to the designed injector linac. The optimisation of the matching section is aimed to make sure that the positron beam is properly transported in the linac, while the optimisation of the initial reference energy is aimed at a maximum final yield. The optimised initial reference energy is 183 MeV, while the optimised matching section are summarised in Table 14. The transport efficiency due to the 20 mm radius aperture of the linac is 98%, while the efficiency due to the PDR energy acceptance and beam length requirement is 87%. The final effective positron yield with the injector linac simulated is 2.14 e^+/e^-, while the normalised PEDD is 31.9 J/g. It should be noticed that the simulated final yield is a bit larger than the calculated yield 2.00 e^+/e^-, where injector linac is not actually simulated. This is actually due to the fact that in the optimisation and calculation of the energy gain of the injector linac, the initial reference energy is fixed to 200 MeV, while in the simulation it is re-optimised to be ~182 MeV, otherwise, they are quite close.

Table 14: Optimised matching section of the injector linac.

Structure	Length [m]	Strength [GeV/m]	Gradient [T/m]	R_{max} at $B_{\text{max}} = 1.2$ T [cm]
Drift	0.211			
Focusing quadrupole	0.4	**0.176**	1.47	81.8
Drift	0.196			
Defocusing quadrupole	0.4	**-0.392**	-3.27	36.7
Drift	0.362			
Focusing quadrupole	0.4	**0.402**	3.35	35.8
Drift	0.495			
Defocusing quadrupole	0.4	**-0.635**	-5.30	22.7
Drift	0.114			

The evolution of the beam size and the normalised RMS beam emittance as a function of the longitudinal position during the transport of the positron beam in the injector linac is presented in Figures 14 and 15, respectively. The normalised RMS beam emittances of the positron beam along X and Y coordinates at the exit of the injector linac are 7.4 mm·rad and 7.9 mm·rad, respectively.

The transverse and longitudinal phase spaces of the output positron beam at the end of the injector linac are presented in Figure 16 and 17, respectively. The cut window for the energy acceptance and beam length requirement by the PDR, as well as positrons beyond and inside the cut window, is also displayed in the plot.
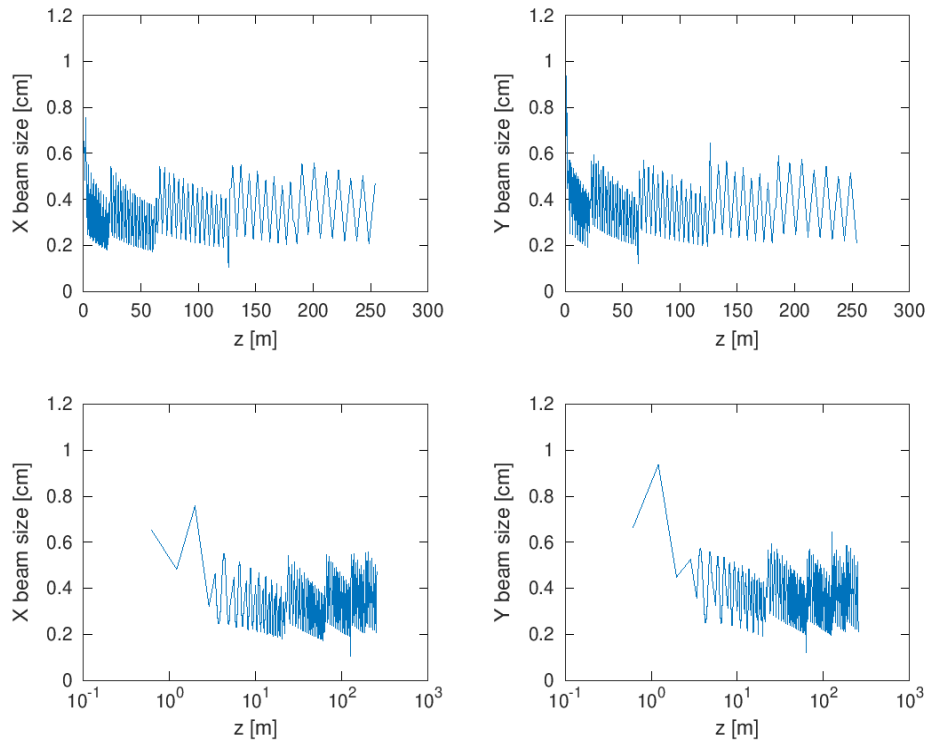
Figure 14: Evolution of the positron beam size as a function of the longitudinal position. The plots are also shown in the log-scale for a better display of the bean size in the matching section.
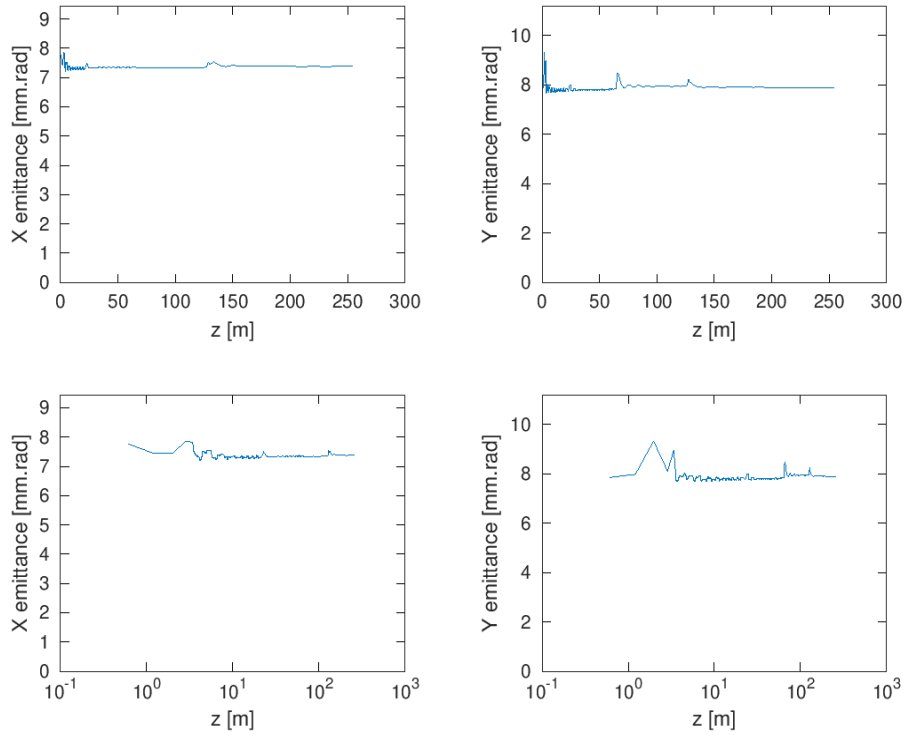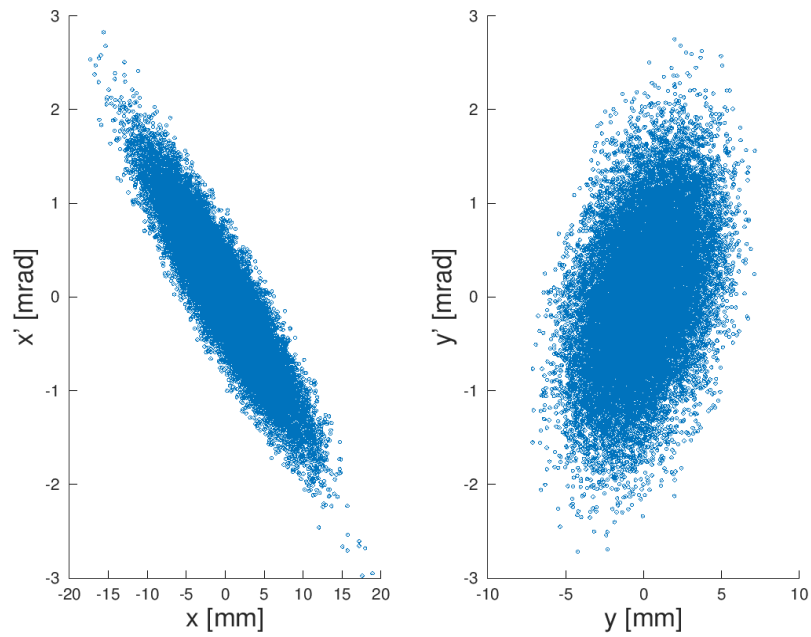
Figure 15: Evolution of the positron normalised RMS beam emittance as a function of the longitudinal position. The plots are also shown in the log-scale for a better display of the bean size in the matching section.

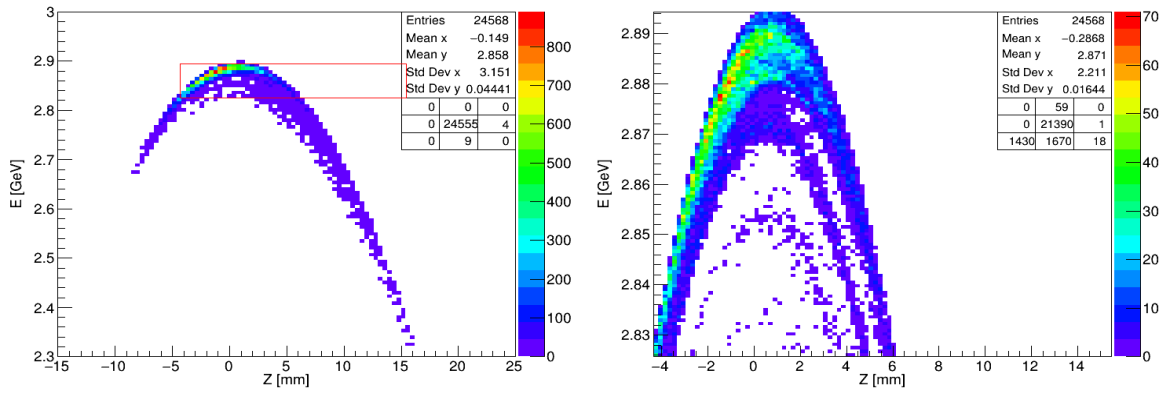Figure 16: Transverse phase spaces of the positron beam at the end of the injector linac.

24

Figure 17: Longitudinal phase space of the positron beam at the end of the injector linac. The left plot shows all the positrons, while the right plot shows the accepted positrons by the PDR. The red box in the left plot corresponds to the energy and beam length window.

8 Summary

In this report, we proposed a new simple, general and effective optimisation strategy for positron source, which is based on iterations of scan of free parameters. The new strategy is faster, simpler and more convincing with results that are visually drawn and can be flexibly tuned, and has the advantage of easily handling realistic parametric problems. The optimisation of the CLIC positron source for the $3\,\mathrm{TeV}$ and $1.5\,\mathrm{TeV}$ stages is presented. As a result, the new optimisation strategy is successfully applied, and satisfying optimised results are obtained as expected. Compared with previous CLIC positron source optimisation method and results, the new developed optimisation strategy can be more than 25 times faster than the old algorithm, and the final effective positron yield is improved by 43%, mainly due to the removal of the distance between the targets. To validate the simulation code, a cross-check is performed to reproduce the ILC positron source results, and a good agreement is observed. In addition, a study is performed to estimate the accepted cubic mesh grid size for energy deposition in PEDD estimation. A general formula is put forward to describe the accepted grid size range as a function of the beam spot size and can be scaled by the number of simulated primary electrons and the primary electron energy. The $0.5\,\mathrm{mm}$ cubic mesh grid size used in this report is well included in the accepted ranges. The latest design of the injector linac is also simulated, and a matching of the positron beam at the exit of the pre-injector linac to the designed injector linac is successfully carried out after a re-optimisation of the positron source. With the re-optimised positron source configuration, positrons are well transported in the injector linac almost without losses, and the final accepted yield by the PDR is $2.14\,e^+/e^-$, while the normalised PEDD is $31.9\,\mathrm{J/g}$.

References

[1] M. Aicheler, P. Burrows, M. Draper, T. Garvey, P. Lebrun, K. Peach, N. Phinney, H. Schmickler, D. Schulte, and N. Toge, *A Multi-TeV Linear Collider Based on CLIC Technology: CLIC Conceptual Design Report*. CERN Yellow Reports: Monographs, Geneva: CERN, 2012.

[2] L. Linssen, A. Miyamoto, M. Stanitzki, and H. Weerts, *Physics and Detectors at CLIC: CLIC Conceptual Design Report*. CERN Yellow Reports: Monographs, Geneva: CERN, 2012. Comments: 257 p, published as CERN Yellow Report CERN-2012-003.

[3] P. Lebrun, L. Linssen, A. Lucaci-Timoce, D. Schulte, F. Simon, S. Stapnes, N. Toge, H. Weerts, and J. Wells, "The CLIC Programme: Towards a Staged e+e- Linear Collider Exploring the Terascale : CLIC Conceptual Design Report," 2012.

[4] M. J. Boland *et al.*, *Updated baseline for a staged Compact Linear Collider*. CERN Yellow Reports: Monographs, Geneva: CERN, Aug 2016. Comments: 57 pages, 27 figures, 12 tables.

[5] M. Aicheler, P. Burrows, N. Catalan Lasheras, R. Corsini, M. Draper, J. Osborne, D. Schulte, S. Stapnes, and M. Stuart, *The Compact Linear Collider (CLIC) Project Implementation Plan*. CERN Yellow Reports: Monographs, Mar 2019. 247 p.

[6] P. Burrows *et al.*, *The Compact Linear Collider (CLIC) - 2018 Summary Report*. CERN Yellow Reports: Monographs, Dec 2018. Published as CERN Yellow Report Monograph Vol. 2/2018.

[7] X. Artru, R. Chehab, M. Chevallier, and V. Strakhovenko, "Advantages of axially aligned crystals used in positron production at future linear colliders," *Phys. Rev. ST Accel. Beams*, vol. 6, p. 091003, 2003.

[8] C. Adolphsen, M. Barone, B. Barish, K. Buesser, P. Burrows, J. Carwardine, J. Clark, H. M. Durand, G. Dugan, E. Elsen, A. Enomoto, B. Foster, S. Fukuda, W. Gai, M. Gastal, R. Geng, C. Ginsburg, S. Guiducci, M. Harrison, H. Hayano, K. Kershaw, K. Kubo, V. Kuchler, B. List, W. Liu, S. Michizono, C. Nantista, J. Osborne, M. Palmer, J. M. Paterson, T. Peterson, N. Phinney, P. Pierini, M. Ross, D. Rubin, A. Seryi, J. Sheppard, N. Solyak, S. Stapnes, T. Tauchi, N. Toge, N. Walker, A. Yamamoto, and K. Yokoya, "The International Linear Collider Technical Design Report," Tech. Rep. arXiv:1306.6328. ANL-HEP-TR-13-20. BNL-100603-2013-IR. IRFU-13-59. Cockcroft-13-10. CERN-ATS-2013-037. CLNS-13-2085. DESY-13-062. FERMILAB-TM-2554. IHEP-AC-ILC-2013-001. ILC-REPORT-2013-040. INFN-13-04-LNF. JAI-2013-001. JINR-E9-2013-35. JLAB-R-2013-01. KEK-Report-2013-1. KNU-CHEP-ILC-2013-1. LLNL-TR-635539. SLAC-R-1004. ILC-HiGrade-Report-2013-003, Geneva, Jun 2013. Comments: See also http://www.linearcollider.org/ILC/TDR . The full list of signatories is inside the Report.

[9] R. Chehab, G. Le Meur, B. Mouton, and M. Renard, "An adiabatic matching device for the orsay linear positron accelerator," *IEEE Transactions on Nuclear Science*, vol. 30, pp. 2850–2852, Aug 1983.

[10] Y. Han, C. Bayar, S. Dbert, A. Latina, L. Ma, and D. Schulte, "Update of the CLIC Positron Source," in *Proceedings, 9th International Particle Accelerator Conference (IPAC 2018): Vancouver, BC Canada, April 29-May 4, 2018*, p. MOPMF055, 2018.

[11] A. Ferrari, L. Rinolfi, and F. A. Tecker, "Design Study of the CLIC Main Beam Injector Linac," Tech. Rep. CERN-OPEN-2005-011. CLIC-Note-626, CERN, Geneva, Apr 2005.

[12] A. Ferrari, L. Rinolfi, and F. A. Tecker, "Particle tracking in the CLIC main beam injector linac," Tech. Rep. CERN-OPEN-2006-015. CLIC-Note-655, CERN, Geneva, Feb 2006.

[13] A. Ferrari, A. Latina, and L. Rinolfi, "Design Study of the CLIC Injector and Booster Linacs with the 2007 Beam Parameters," May 2008.

[14] A. Vivoli, I. Chaikovska, R. Chehab, O. Dadoun, P. Lepercq, F. Poirier, L. Rinolfi, V. Strakhovenko, and A. Variola, "The CLIC Positron Capture and Acceleration in the Injector Linac.," Tech. Rep. CERN-OPEN-2010-020. CLIC-Note-819, CERN, Geneva, Jun 2010.

[15] C. Bayar, A. Ciftci, S. Doebert, and A. Latina, "Design and optimisation of the positron production chain for clic from the target to the damping ring," *Nuclear Instruments and Methods in Physics Research Section A: Accelerators, Spectrometers, Detectors and Associated Equipment*, vol. 869, pp. 56 – 62, 2017.

[16] S. Agostinelli *et al.*, "GEANT4: A Simulation toolkit," *Nucl. Instrum. Meth.*, vol. A506, pp. 250–303, 2003.

[17] A. Xavier, "A simulation code for channeling radiation by ultrarelativistic electrons or positrons," *Nuclear Instruments and Methods in Physics Research Section B: Beam Interactions with Materials and Atoms*, vol. 48, no. 1, pp. 278 – 282, 1990.

[18] A. Latina, "RF-Track: Beam tracking in field maps including space-charge effects, features and benchmarks," p. MOPRC016. 4 p, 2017. 28th Linear Accelerator Conference, East Lansing, Michigan, 25 - 30 Sep 2016.

[19] R. H. Helm, "ADIABATIC APPROXIMATION FOR DYNAMICS OF A PARTICLE IN THE FIELD OF A TAPERED SOLENOID," 1962. SLAC report: SLAC-R-004.

[20] H. Nagoshi, "A design study of the electron-driven ilc positron source." International Workshop on Future Linear Colliders, 22-26 October 2018.

[21] M. Fukuda, "A yield calculation for e-driven ilc positron source." International Workshop on Future Linear Colliders, 22-26 October 2018.

[22] Y. Zhao, "A new simple strategy for clic positron source optimisation." International Workshop on Future Linear Colliders, 28 October - 1 November 2019.

[23] Y. Han, C. Bayar, A. Latina, S. Doebert, D. Schulte, and L. Ma, "Optimization of the clic positron source using a start-to-end simulation approach involving multiple simulation codes," *Nuclear Instruments and Methods in Physics Research Section A: Accelerators, Spectrometers, Detectors and Associated Equipment*, vol. 928, pp. 83 – 88, 2019.

[24] J. A. Nelder and R. Mead, "A Simplex Method for Function Minimization," *The Computer Journal*, vol. 7, pp. 308–313, 01 1965.

[25] D. Freedman and P. Diaconis, "On the histogram as a density estimator: L_2 theory," *Probability Theory and Related Fields*, vol. 57, pp. 453–476, 12 1981.

[26] D. Schulte, "PLACET: A program to simulate drive beams," in *7th European Particle Accelerator Conference (EPAC 2000)*, pp. 1402–1404, 7 2000.